19th Brazilian Congress of Thermal Sciences and Engineering
November 6th–10th, 2022, Bento Gonçalves - RS - Brazil

ENC-2022-0437
ESTIMATION OF HEAT CONVECTION COEFFICIENT IN A SOLID PROPELLANT ROCKET MOTOR NOZZLE

Arthur Mendonça de Azevedo
Elisan dos Santos Magalhães
Instituto Tecnológico da Aeronáutica – ITA, Pç Mal. Eduardo Gomes 50, São José dos Campos, SP, 12228-900, Brazil
arthurama@ita.br
elisan@ita.br

Humberto Araujo Machado
Instituto de Aeronáutica e Espaço – IAE, Pç Mal. Eduardo Gomes 50, São José dos Campos, SP, 12228-904, Brazil
Faculdade de Tecnologia – FAT/UERJ, Rod. Pres. Dutra km 298, Resende, RJ, 27537-000, Brazil
humbertoham@fab.mil.br

Abstract. *During the gas flow inside a rocket nozzle, it is essential to estimate the internal wall heat flux to assure that the nozzle structure can resist the heat load. The convection coefficient between the gas and the wall can be estimated through the Bartz equation and then used to obtain the temperature profile in the nozzle wall. The Bartz equation is employed in this work to estimate the heat convection coefficient and the resulting temperature field in the S-30 rocket nozzle. A sensibility analysis is performed to verify the equation accuracy, and the numerical results are compared with experimental measurements, presenting coherent results. The methodology proved to be applicable for the nozzle structure dimensioning.*

Keywords: *rocket nozzle, Bartz equation, sensibility analysis, heat convection coefficient*

1. INTRODUCTION

The Institute of Aeronautics and Space (IAE) has been responsible for developing the vehicles of the Brazilian Space Program for the last 40 years, which employ solid-propellant rocket engines. The propellant burns in a combustion chamber and the resulting gases are expelled through a nozzle to boost the vehicle. Since the gas is expelled at a high temperature, this is necessary to estimate the heat transfer in the wall to assure that the nozzle structure will be able to resist the thermal and dynamic loads. Inside the nozzle, the primary heat sources are the convection from the gas and the radiation from the alumina particles that flow along and are produced by the combustion of the aluminum added to the propellant. The most accurate way to calculate the convection within the nozzle is through CFD (Computation Fluid Dynamics), which implies high computational effort and time-demanding. An alternative way is using an engineering method, applying empirical equations to estimate the heat convection coefficient. In most cases, this is enough to obtain satisfactory results for nozzle evaluation. This work applied the Bartz equation (Bartz, 1957) to estimate the heat convection coefficient. Then, the nozzle's axial direction's temperature, pressure, and velocity are obtained through the one-dimension perfect gas approach. Once the convection coefficient and temperature in the nozzle wall are available, these data are applied as boundary conditions in a CFD program to estimate the temperature profiles in the wall. Finally, the authors compared the simulation results with the experimental data extracted from a rocket engine test at IAE, presenting qualitative coherence and valuable information for a rocket nozzle design.

2. METHODOLOGY

2.1 One-dimensional profiles of temperature, pressure, and flow velocity along the axis of the S-30 rocket engine nozzle

Fig. 1 shows the S-30 rocket engine nozzle, a converging/diverging nozzle. Considering isentropic flow in the converging/diverging nozzle allows assuming that the stagnation temperature and pressure are constant along the nozzle axis (Fox *et al.*, 2014). Thus, based on the thermodynamic state of the rocket engine combustion chamber,

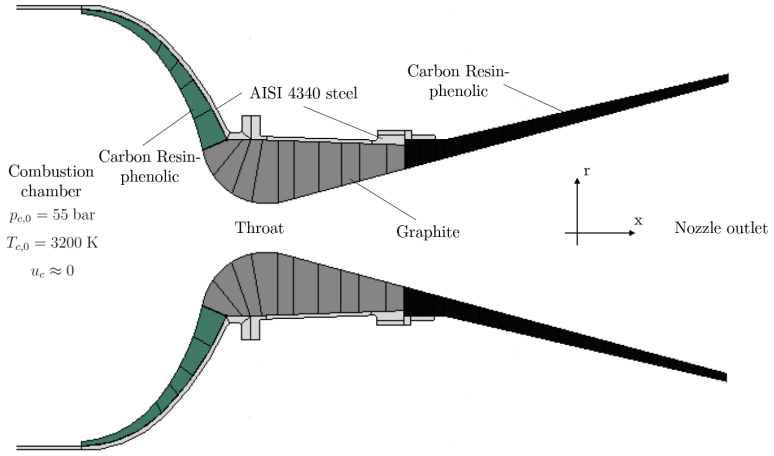

Figure 1: S-30 rocket engine nozzle scheme.

$$T_{\text{flow}} = \frac{T_{c,0}}{1 + \dfrac{\gamma - 1}{2} M^2} \tag{1}$$

$$p_{\text{flow}} = p_{c,0} \left(\frac{T_{\text{flow}}}{T_{c,0}} \right)^{\frac{\gamma}{\gamma - 1}} \tag{2}$$

$$u_{\text{flow}} = M \sqrt{\gamma R_g T_{\text{flow}}} \tag{3}$$

where T_{flow} is the flow static temperature, p_{flow} is the flow static pressure, u_{flow} is the flow static velocity, $T_{c,0}$ is the combustion chamber stagnation temperature, $p_{c,0}$ is the combustion chamber stagnation pressure, γ is the gas adiabatic expansion coefficient, M is the Mach number, and R_g is the gas constant.

This work determined the Mach number from the following transcendental equation,

$$\frac{A}{A_t} = \frac{1}{M} \left(\frac{1 + \dfrac{\gamma - 1}{2} M^2}{\dfrac{\gamma + 1}{2}} \right)^{\frac{\gamma + 1}{2(\gamma - 1)}} \tag{4}$$

where A is the cross-sectional area along the nozzle, and A_t is the throat sectional area.

2.2 Bartz's correlation to determine the convection heat transfer coefficient inside the nozzle

Bartz's correlation can be expressed by (Bartz, 1957),

$$h_{\text{Bartz},i} = \left[\frac{0.026}{D_{t,i}^{0.2}} \left(\frac{\mu^{0.2} \cdot C_{p,i}}{Pr^{0.6}} \right) \left(\frac{p_{c,0,i} \cdot g_i}{c_i^*} \right)^{0.8} \left(\frac{D_{t,i}}{r_{t,i}} \right)^{0.1} \right] \left(\frac{A_{t,i}}{A_i} \right)^{0.9} \sigma_{c,i} \quad [\text{BTU/s } ^{\text{o}}\text{F in}^2] \tag{5}$$

where $h_{\text{Bartz},i}$ is the Bartz convection heat transfer coefficient, $D_{t,i}$ is the throat diameter, μ is the gas viscosity, Pr is the gas Prandtl number, g_i is the gravity acceleration, c_i^* is the characteristic velocity, and $\sigma_{c,i}$ is the correction parameter. The characteristic velocity (c_i^*) measures rocket engine combustion performance independent of nozzle performance (Sutton and Biblarz, 2010). Eq. (5) presents its original form, i.e., the variables data are in the British system of units. The subscript i indicates this. Then, Tab. 1 shows all necessary unit conversions used in the calculation of Eq. (5).

The gas viscosity can be written as (Bartz, 1957),

$$\mu = 46.6 \times 10^{-10} (\overline{m})^{0.5} (T_{\text{flow,i}})^{0.6} \quad [\text{lb/in sec}] \tag{6}$$

where $\overline{m}$ is the combustion gas average molar mass. The correction parameter is given by (Bartz, 1957),

$$\sigma_{c,i} = \left\{ \left[\frac{T_{w,i}}{2T_{c,0,i}} \left(1 + \frac{\gamma - 1}{2} M^2 \right) + 0.5 \right]^{0.68} \left(1 + \frac{\gamma - 1}{2} M^2 \right)^{0.12} \right\}^{-1} \tag{7}$$

where $T_{w,i}$ is the nozzle internal wall temperature. Finally, to obtain h_{Bartz}, in the S.I. system of units,

$$h_{\text{Bartz}} = 5.6782 \times 3600 \times 144 \times h_{\text{Bartz,i}} \quad [\text{W/m}^2\text{K}] \tag{8}$$

Table 1: Conversion between the British and S.I. system of units.

S.I. system of units	British system of units
r_t [m]	$r_{t,i}$ [in] $= 39.3701 \times r_t$ [m]
D_t [m]	$D_{t,i}$ [in] $= 39.3701 \times D_t$ [m]
A [m^2]	A_i [in^2] $= (39.3701)^2 \times A$ [m^2]
	$[\overline{m}]$ = g/mol
T [K]	T_i [^{o}R] $= 1.8 \times T$ [K]
C_p [J/kgK]	$C_{p,i}$ [BTU/lb ^{o}F] $= 2.3884 \times 10^{-4} \times C_p$ [J/kgK]
	$Pr = \frac{4\gamma}{9\gamma - 5}$
$p_{c,0}$ [Pa]	$p_{c,0,i}$ [lb/in^2] $= 1.4503 \times 10^{-4} \times p_{c,0}$ [Pa]
g [m/s^2]	g_i [ft/s = fps^2]^2 $= 3.2808 \times g$ [m/s^2]
c^* [m/s]	c_i^* [ft/s = fps] $= 3.2808 \times c^*$ [m/s]

2.3 Mathematical model of the S-30 rocket engine thermal analysis

The phenomenon of heat transfer along the S-30 engine nozzle and in its radial direction, when submitted to the "bench shot" test, can be mathematically modeled through the transient one-dimensional heat diffusion equation, given as:

$$\frac{\partial}{\partial r}\left(k\frac{\partial T}{\partial r}\right) + S = \rho C_p \frac{\partial T}{\partial t} \tag{9}$$

where k is the material thermal conductivity, T is the material temperature, r is the one-dimensional rectangular coordinate, S is the heat source, ρ is the material density, C_p is the specific heat, and t is the time. Fig. 2 presents, in red color, an example of the one-dimensional mesh direction for the rocket engine thermal analysis.

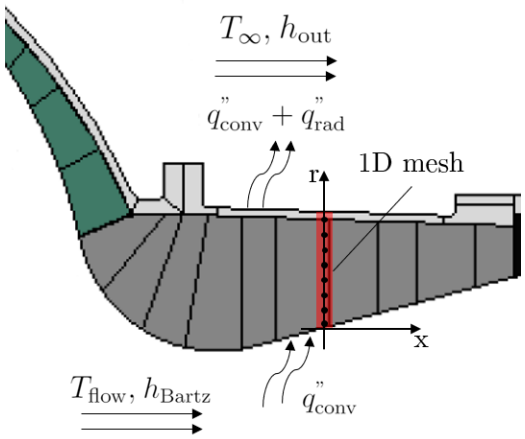

Figure 2: One-dimensional mesh for the S-30 rocket engine thermal analysis.

The initial and boundary conditions can be given as,

$$T(r, t = 0) = T_0 \tag{10}$$

$$k\frac{\partial T}{\partial r}\bigg|_{r=0} = h_{\text{Bartz}}(T_{\text{flow}} - T) \tag{11}$$

$$k\frac{\partial T}{\partial r}\bigg|_{r=L} = h_{\text{out}}(T - T_\infty) + \varepsilon\sigma(T^4 - T_\infty^4) \tag{12}$$

where T_0 is the nozzle initial temperature, h_{out} is the natural convection heat transfer coefficient at the outside, T_∞ is the environment temperature, ε is the material emissivity, σ is the Stefan-Boltzmann constant, and L is the mesh length.

2.4 Numerical model

This paper applied the Finite Volume Method (FVM) for solving the mathematical model represented in Eq. (9). In this method, the energy conservation balance on the elementary control volume (CV) results in approximated equations.

Fig. 2 shows the one-dimensional CV (dashed rectangle). The point P indicates the central node of the CV, and the points E and W indicate its neighboring nodes to the east and west, respectively. The indications e and w, in turn, represent the boundaries of the CV to the east and west, respectively.

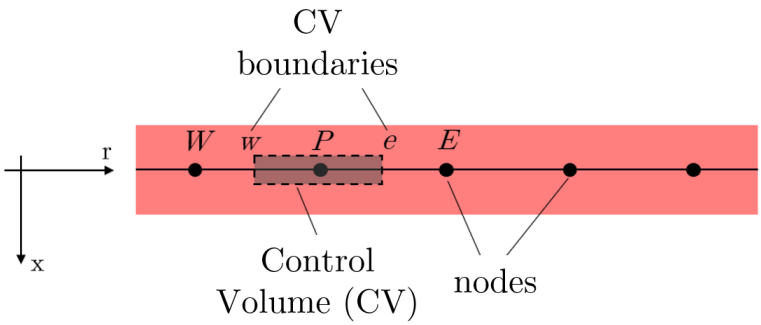

Figure 3: One-dimensional uniform mesh of Fig. 2.

Integrating the result into the time, from t to $t + \Delta t$, and into the CV of Fig. 2, the linear system of the numerical model can be written as:

$$a_{_P} T_{_P}^{p+1} = a_{_E} T_{_E}^{p+1} + a_{_W} T_{_W}^{p+1} + b \tag{13}$$

where,

$$a_{_E} = \frac{k}{\Delta r}, \qquad a_{_W} = \frac{k}{\Delta r} \tag{14}$$

$$a_{_P} = a_{_E} + a_{_W} + +\rho C_p \frac{\Delta r}{\Delta t} \tag{15}$$

$$b = S + \rho C_p \frac{\Delta r}{\Delta t} T_{_P}^{p} \tag{16}$$

where a is the coefficients, b is the total source term, Δr is the CV length, Δt is the time step, and the superscript p is the time step counter.

Eq. (13) composes a equation system with dimension equal at the mesh size. Eq. (17), a tridiagonal matrix, represents an example of this system. The authors implemented the Parallel Cyclic Reduction (PCR) algorithm for the tridiagonal matrix solution. PCR is the most efficient algorithm for this case. Furthermore, as it is a Parallel Reduction, this work used a GPU (Graphics Processing Unit) to solve the heat transfer problem.

$$\begin{bmatrix} a_{p,1} & a_{e,1} & 0 & \cdots & 0 \\ a_{w,2} & a_{p,2} & a_{e,2} & \ddots & \vdots \\ 0 & a_{w,3} & a_{p,3} & \ddots & 0 \\ \vdots & \ddots & \ddots & \ddots & a_{e,n-1} \\ 0 & \cdots & 0 & a_{w,n} & a_{p,n} \end{bmatrix} \begin{bmatrix} T_1^{p+1} \\ T_2^{p+1} \\ T_3^{p+1} \\ \vdots \\ T_n^{p+1} \end{bmatrix} = \begin{bmatrix} b_1 \\ b_2 \\ b_3 \\ \vdots \\ b_n \end{bmatrix} \tag{17}$$

3. Materials and flow properties

The S-30 rocket engine nozzle is composed of different materials, such as carbon resin-phenolic (C-phenolic) and graphite, and steel (Fig. 1). The first two are responsible for supporting the gas high temperatures of the solid propellant burning. Tab. 2 shows the thermal properties of the S-30 rocket engine nozzle materials. For the gas flow properties, throat data, initial and boundary conditions, this paper considered the data in Tab. 3.

4. RESULTS AND DISCUSSION

4.1 Mesh convergence analysis

This work considered a simple case to test the one-dimensional uniform mesh and the numerical solution performance. Fig. 4a presents a thin plate of thickness $L = 0.02$ m and an initial uniform temperature of 200 °C. At the eastern end of

Table 2: Thermophysical properties of the S-30 rocket engine nozzle materials.

Property	**Material**			
	Graphite	C-phenolic	AISI 4340 steel	Glue
Thermal conductivity [W/mK]	150	4.0	16.2	5.9
Density [kg/m^3]	1810	1700	8000	1700
Specific heat at constant pressure [J/kgK]	837.5	1300	500	1300
Emissivity	0.8	0.97	0.11	-

Table 3: Flow properties, throat data, and initial and boundary conditions.

Property	**Value**
Throat position	$x_t = 0.05480$ m
Throat radius	$r_t = 0.07168$ m
Combustion chamber stagnation temperature	$T_{c,0} = 3200.0$ K
Combustion chamber stagnation pressure	$p_{c,0} = 55$ bar
Gas constant	$R_g = 332.57$ J/kgK
Adiabatic expansion coefficient	$\gamma = 1.1509$
Specific heat at constant pressure	$C_{p,\text{flow}} = 1995.4$ J/kgK
Combustion gas average molar mass	$\overline{m} = 24.5671$ g/mol
Material initial temperature	$T_0 = 295.0$ K
Environment temperature	$T_\infty = 295.0$ K
Convection heat transfer coefficient at outside	$h_{\text{out}} = 6.0$ W/m^{2}K
Stefan-Boltzmann constant	$\sigma = 5.6704 \times 10^{-8}$ W/m^{2}K^4

the grid, this case considered the prescribed temperature $T_E = 0$ °C from the instant $t = 0$ s. The west end, in turn, was isolated. Thermal conductivity of the material was assumed $k = 10$ W/mK and $\rho C_p = 10 \times 10^6$ J/m^{3}K, in addition to the time interval $\Delta t = 0.01$ s.

The analytical solution for this case is given as follows (Necati, 1985),

$$T(x,t) = \frac{800}{\pi} \sum_{n=1}^{\infty} \frac{(-1)^{n+1}}{2n-1} e^{-\frac{k}{\rho C_p}\lambda_n^2 t} \cos(\lambda_n x) \tag{18}$$

where,

$$\lambda_n = \frac{(2n-1)\pi}{2L} \tag{19}$$

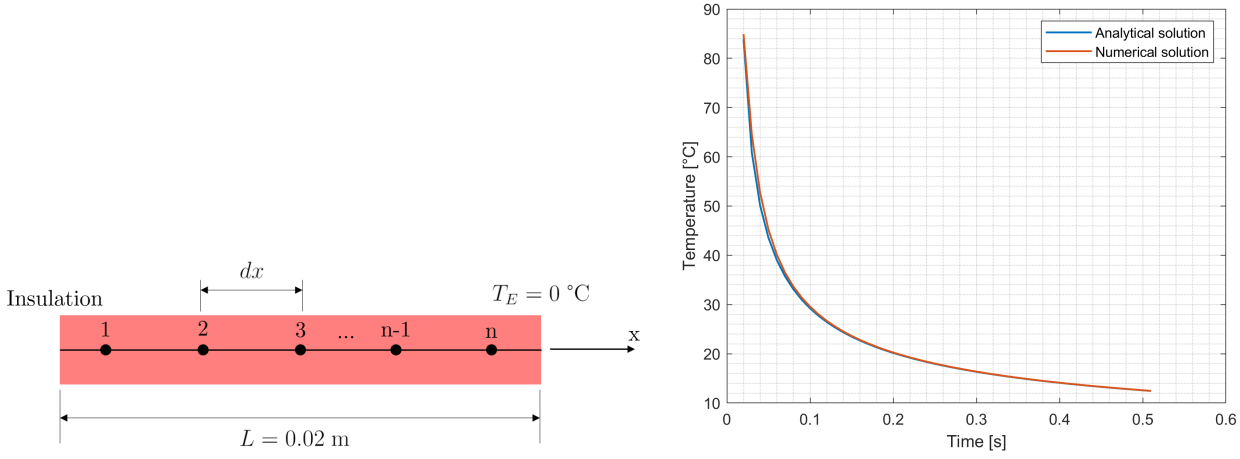

(a) One-dimensional test scheme.

(b) Simulation with a 128 CV's mesh.

Figure 4: Uniform mesh convergence test.

A mesh size independence study has concluded that the outputs became independent of grid refinement at 128 CV's. Fig. 4b presents the analytical and the numerical solutions.

4.2 Comparisons between the direct method numerical simulations and the experimental results

The thermocouples temperatures positioned at the points of Fig. 5 were obtained from the numerical model solution. For the solution of the direct numerical method, this work considered the following: the materials' thermal properties presented in Tab. 2; the sample time $\Delta t = 0.01$ s; the flow profiles (temperature, pressure, and velocity) obtained from Eqs. (1)-(4) with the data presented in Tab. 3; the heat transfer coefficient inside the nozzle, obtained from Eq. (5), and the uniform mesh with 128 CV's.

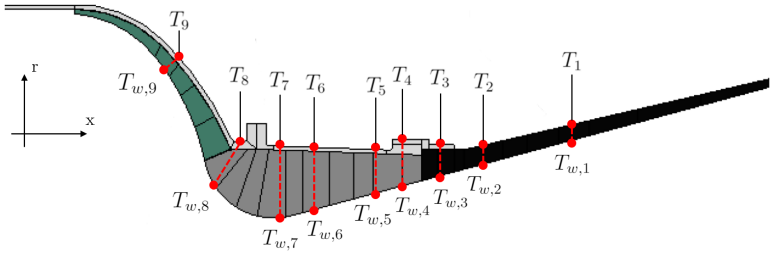

Figure 5: Positioning of thermocouples on the external surface of the S-30 motor nozzle and directions of the one-dimensional meshes.

For the comparisons between the numerical solution and the experimental data, the authors presented the thermocouples results for T_1, T_2, T_3 and T_8 positions. Figs. 6a-6d show these results.

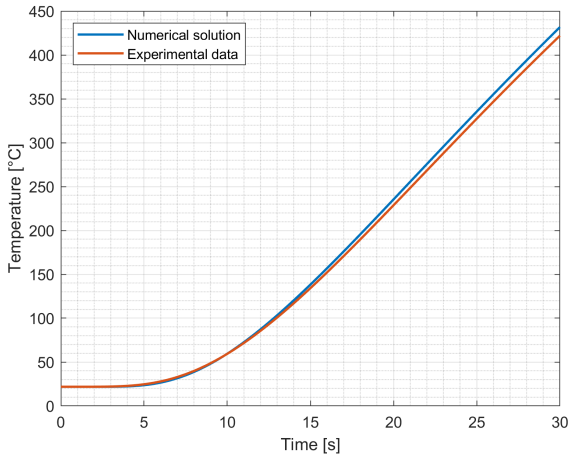

(a) Thermocouple T_1.

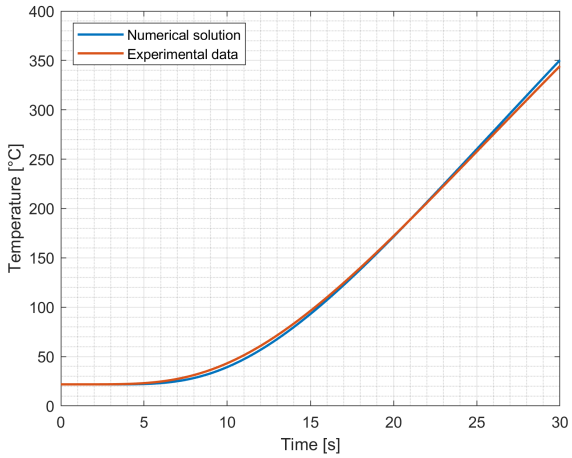

(b) Thermocouple T_2.

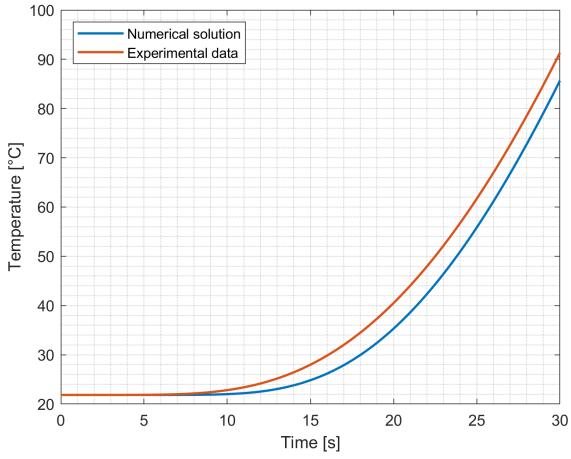

(c) Thermocouple T_3.

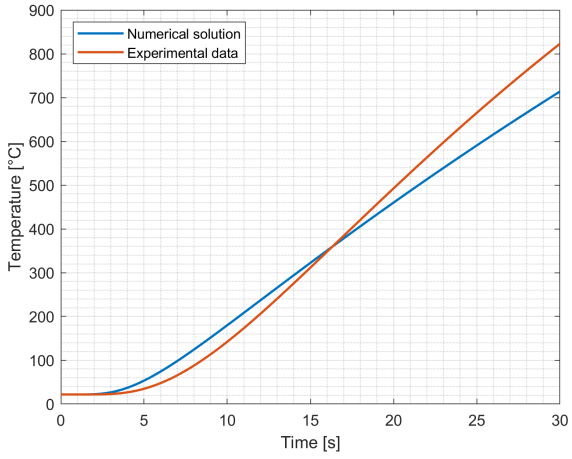

(d) Thermocouple T_8.

Figure 6: Comparisons between the numerical and experimental results.

These results showed a good agreement between the sensor measurements and the proposed numerical model. However, thermocouples 3, and 8, were the most diverged from the expected. The simulation of sensor 3 showed smoother

behavior and a lower heating rate than expected. The simulated sensor 8, in turn, detected rapid initial heating and did not show the same trend as the experimental results. On the other hand, the simulations of sensors 1 and 2 were considered satisfactory and agreed with the experiment. Considering the numerical model chosen, the complexity of the problem requires a two-dimensional treatment for at least the central region of the nozzle, composed of Graphite and AISI 4340 Steel. The two-dimensional numerical model would better detect the temperature gradients induced in the nozzle body by the flue gas flow. Given the similarity with the classical heat conduction problem in long and thin plates, the smaller thicknesses of the thermocouple regions 1 and 2 favor the one-dimensional treatment. Therefore most significant temperature gradient could be detected in the same direction as the thickness.

The consideration of an isentropic flow also contributed to the observed divergences. The nature of the propellant used in the S-30 engine, alumina particles (Al_2O_3), contribute approximately 28% of the molar mass of the gas. Its presence characterizes a two-phase flow of the gas that directly influences the heat transfer of this gas with the structure of the nozzle. In addition, inaccuracies in the positioning of thermocouples and the dimensions of the nozzle present a significant source of errors, compromising a good representation of the numerical model.

5. Sensibility analysis of the Bartz's correlation

The first analysis was to verify Bartz's correlation sensibility with the nozzle internal wall temperature (T_w). Therefore, the authors simulated the nine positions indicated by $T_{w,i}$ com $i = 1$ to 9 in Fig. 5. Fig. 7 presents this analysis. The T_w variation is significant for the estimation of the h_{Bartz} in the regions of thermocouples 4, 5, 6, 7, and 8.

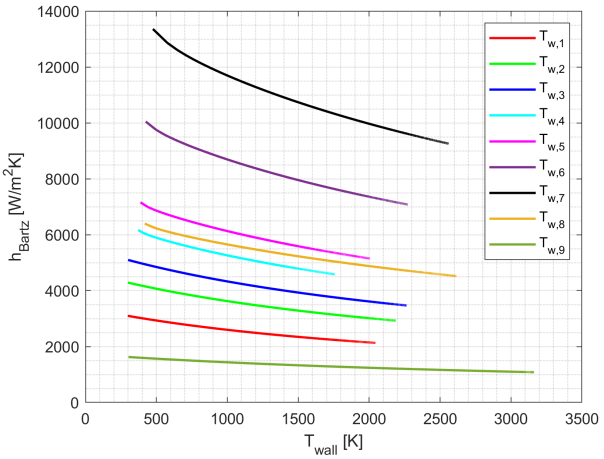

Figure 7: h_{Bartz} sensibility with T_w.

The following analysis focused on the combustion gas properties variations. Then work tested properties such as viscosity, Prandtl number, specific heat, gas constant, and adiabatic expansion coefficient. Nonetheless, h_{Bartz} is a function of T_w. Then, the authors considered two variations for T_w: constant value ($T_w = 300$ K) and the mean between this constant and the temperature of the flow at the outlet of the nozzle ($T_w = 0.5 \times (300 + T_{\text{flow,out}})$). Tab. 4 presents all test cases simulated and analyzed, and Figs. 8a–8e present the Bartz's sensibility results. The following topics highlighted principal conclusions for the sensibility analysis:

- Viscosity analysis – Fig. 8a: constant viscosity showed a subtle change in h_{Bartz} in the region close to the throat and at the nozzle outlet. Thus, h_{Bartz} is not sensitive to variations in gas viscosity since T_w was considered constant.
- Prandtl number – Fig. 8b: There is a relative sensitivity, in the throat region, of h_{Bartz} with Pr. The blue and purple curves show, at $x = 0.0538$ m, 713.6 W/m^{2}K and 629.8 W/ $textm^2$K, respectively, difference of h_{Bartz} compared to the other two curves. Thus, the authors concluded that h_{Bartz} was not sensitive to the Prandtl number.
- Specific heat – Fig. 8c: h_{Bartz} presents considerable sensitivity with the change of C_p, in the throat region. The h_{Bartz} variation was 1766.8 W/m^{2}K and 1559.1 W/m^{2}K, in $x = 0.0538$ m, in the curves for the two cases $T_w = 300$ K and $T_w = 961.28$ K, respectively.
- Gas constant – Fig. 8d: h_{Bartz} is also not very sensitive to variations in the gas constant. In the throat region, the Bartz's coefficient was differences of 761.0 W/m^{2}K and 671.5 W/m^{2}K, for the two cases $T_w = 300$ K and $T_w = 961.28$ K, respectively.
- Adiabatic expansion coefficient – Fig. 8e: There is a minimal variation in h_{Bartz} with γ, given $T_w = 300$ K. However, for the other cases, the change in γ resulted in a small change in T_w of 156.17 K, which in turn promoted

the difference in h_{Bartz} between the two curves of 400.7 W/ m^{2}K at position $x = 0.0538$m (throat region). Thus, the variation of γ will make h_{Bartz} sensitive depending on the approach taken for T_w.

Table 4: Sensibility analysis cases

Gas property analized	**Assumed values**	**Other constant gas properties**
Viscosity	$\mu = \mu(T_{\text{flow}})$ (Eq. (6))	$Pr = \frac{4\gamma}{9\gamma-5}$ $C_p = 1995.4$ J/kgK $R_g = 287.0$ J/kgK $\gamma = 1.1509$
	$\mu = 7 \times 10^{-5}$ Pa $\cdot$ s	
Prandtl number	$Pr = \frac{4\gamma}{9\gamma-5}$	$\mu = 7 \times 10^{-5}$ Pa $\cdot$ s $C_p = 1995.4$ J/kgK $R_g = 287.0$ J/kgK $\gamma = 1.1509$ $k = 0.149$ W/mK $\mu(T_{\text{flow}})$ (Eq. (6))
	$Pr = \frac{\mu C_p}{k}$	
	$Pr = \frac{\mu(T_{\text{flow}})C_p}{k}$	
Specific heat	$C_p = 1995.4$ J/kgK	$Pr = \frac{\mu C_p}{k}$ $\mu = 7 \times 10^{-5}$ Pa $\cdot$ s $k = 0.149$ W/mK $R_g = 287.0$ J/kgK $\gamma = 1.1509$
	$C_p = 2726.0$ J/kgK (air at $T = 3000$ K)	
Gas constant	$R_g = 287.0$ J/kgK	$Pr = \frac{\mu C_p}{k}$ $\mu = 7 \times 10^{-5}$ Pa $\cdot$ s $k = 0.149$ W/mK $C_p = 1995.4$ J/kgK $\gamma = 1.1509$
	$R_g = 332.57$ J/kgK	
Adiabatic expansion coefficient	$\gamma = 1.1509$	$Pr = \frac{\mu C_p}{k}$ $\mu = 7 \times 10^{-5}$ Pa $\cdot$ s $k = 0.149$ W/mK $R_g = 287.0$ J/kgK $C_p = 1995.4$ J/kgK
	$\gamma = 1.2$	

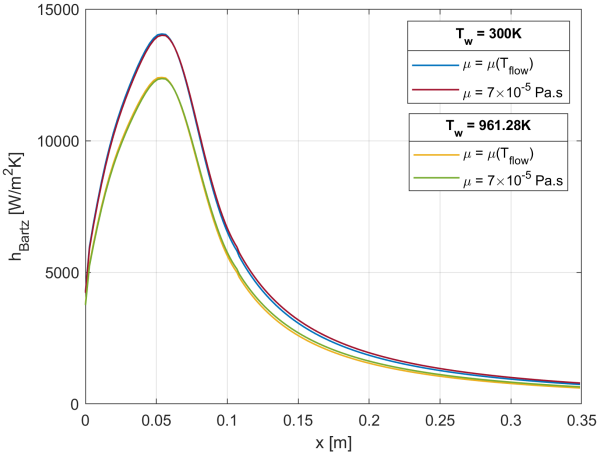

(a) Viscosity.

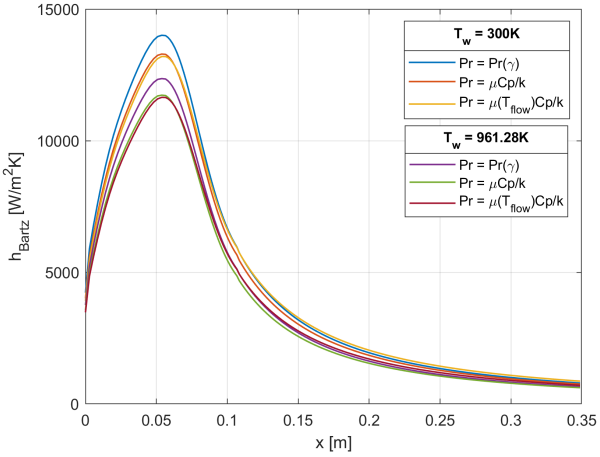

(b) Prandtl number.

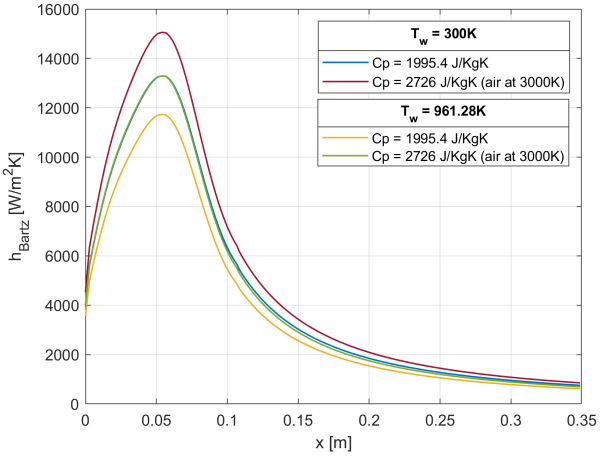

(c) Specific heat.

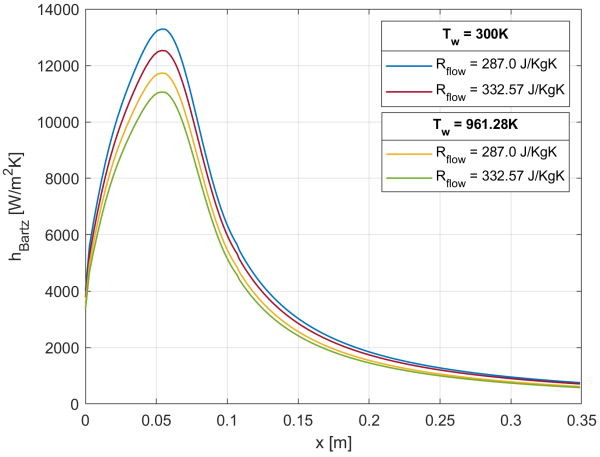

(d) Gas constant.

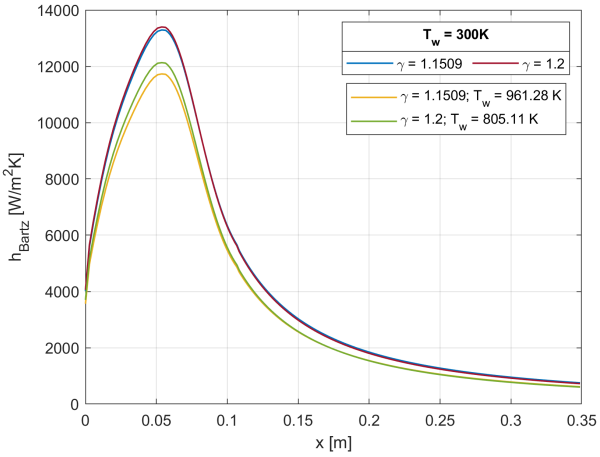

(e) Adiabatic expansion coefficient.

Figure 8: h_{Bartz} sensibility with the combustion gas properties.

6. CONCLUSIONS

First, the results demonstrated that the one-dimensional numerical model achieved satisfactory results in regions of smaller thickness, compared to the length, as observed in Fig. 6a and 6b. However, for the other measurement regions, the two-dimensional treatment of the longitudinal section of the nozzle proved to be necessary.

Finally, the Bartz heat transfer coefficient, in turn, was sensitive to variations in the temperature of the internal nozzle

wall, especially in the throat region. So then, the consideration of T_w as a temperature function is an important parameter when applying h_{Bartz}. In addition, concerning the flue gas parameters, the sensibility analysis brought actual results for future choices of parameters to be considered in the studies.

7. REFERENCES

Bartz, D.R., 1957. "A simple equation for rapid estimation of rocket nozzle convective heat transfer coefficients". *Journal of Jet Propulsion*, Vol. 27, pp. 49–53.

Fox, R.W., MacDonald, A.T. and Leylegian, J.C., 2014. *Introduction to Fluid Mechanics*. LTC, 8th edition. ISBN 9780471775874,0471775878.

Necati, O.M., 1985. *Heat Transfer: A Basic Approach*. McGraw-Hill Book Company. ISBN 007-047982-8.

Sutton, G.P. and Biblarz, O., 2010. *Rocket Propulsion Elements*. Wiley, 8th edition. ISBN 0470080248,9780470080245.

8. RESPONSIBILITY NOTICE

The authors are responsible only for the printed material included in this paper.